

GA-A26068

**EFFECT OF PARTICLE TRANSPORT ON
THE MEASURED ELECTRON CYCLOTRON
CURRENT DRIVE PROFILE**

by

**C.C. PETTY, M.E. AUSTIN, J. LOHR, T.C. LUCE,
M.A. MAKOWSKI, R. PRATER, R.W. HARVEY, and A.P. SMIRNOV**

MAY 2008



DISCLAIMER

This report was prepared as an account of work sponsored by an agency of the United States Government. Neither the United States Government nor any agency thereof, nor any of their employees, makes any warranty, express or implied, or assumes any legal liability or responsibility for the accuracy, completeness, or usefulness of any information, apparatus, product, or process disclosed, or represents that its use would not infringe privately owned rights. Reference herein to any specific commercial product, process, or service by trade name, trademark, manufacturer, or otherwise, does not necessarily constitute or imply its endorsement, recommendation, or favoring by the United States Government or any agency thereof. The views and opinions of authors expressed herein do not necessarily state or reflect those of the United States Government or any agency thereof.

EFFECT OF PARTICLE TRANSPORT ON THE MEASURED ELECTRON CYCLOTRON CURRENT DRIVE PROFILE

by

C.C. PETTY, M.E. AUSTIN,* J. LOHR, T.C. LUCE,
M.A. MAKOWSKI,† R. PRATER, R.W. HARVEY,‡ and A.P. SMIRNOV‡

*University of Texas at Austin, Austin, Texas

†Lawrence Livermore National Laboratory, Livermore, California

‡CompX, Del Mar, California

This is a preprint of an invited paper to be presented at the 15th Joint Workshop on Electron Cyclotron Emission and Electron Cyclotron Resonance Heating to be held in Yosemite National Park, California on March 10–13, 2008 and to be published in the Proceedings.

Work supported by
the U.S. Department of Energy
under DE-FC02-04ER54698, DE-FG03-97ER54415,
DE-FG03-99ER54541 and DE-AC52-07NA27344

GENERAL ATOMICS PROJECT 30200
MAY 2008



EFFECT OF PARTICLE TRANSPORT ON THE MEASURED ELECTRON CYCLOTRON CURRENT DRIVE PROFILE*

C. C. PETTY,[†] J. LOHR, T. C. LUCE AND R. PRATER
General Atomics, P.O. Box 85608, San Diego, California 92186-5608, USA

R. W. HARVEY AND A. P. SMIRNOV
CompX, P.O. Box 2672, Del Mar, California 92014-5672, USA

M. E. AUSTIN
*University of Texas at Austin, Fusion Research Center, College of Natural Sciences,
1 University Station C1510, Austin, Texas 78712, USA*

M. A. MAKOWSKI
*Lawrence Livermore National Laboratory, 7000 East Avenue, Livermore,
California 94550, USA*

Radial transport of the current carrying electrons can broaden the profile of electron cyclotron current drive (ECCD), with potentially detrimental effects for applications that rely on strong localization of the noninductive current. Early experiments on the DIII-D tokamak did not observe any clear effects of particle transport on the ECCD profile. However, more recent experiments at high ECCD power, low density, and radiation temperatures above 20 keV clearly demonstrate that the ECCD profile is reduced and broadened compared to CQL3D predictions assuming no radial transport. At high relative power densities, a diffusion coefficient of $\approx 0.4 \text{ m}^2/\text{s}$ is required in CQL3D to reproduce the experimental ECCD profile, while smaller diffusion coefficients are needed to model the ECCD profile at low relative power densities. This level of transport is an order of magnitude less than the electron thermal diffusivity but is comparable to the effective particle transport rate needed to maintain the density profile.

1. Introduction

There are several important applications on ITER for the localized noninductive current generated by electron cyclotron (EC) waves, including the suppression

* This work was supported by the US Department of Energy under DE-FC02-04ER54698, DE-FG03-97ER54415, DE-FG03-99ER54541, and DE-AC52-07NA27344.

[†] e-mail: petty@fusion.gat.com

of neoclassical tearing modes (NTM) [1]. While the strong absorption of EC waves guarantees that the power deposition is localized along the ray path, radial transport of the current carrying electrons can make the resulting current drive profile significantly broader than the deposition profile. Owing to the inverse scaling of transport with plasma size, the effects of radial transport on ECCD are expected to be stronger in smaller devices. For example, studies on the TCV tokamak showed that quasi-linear Fokker-Planck modeling could be brought in line with ECCD measurements only by including radial transport at levels similar to the thermal energy transport [2]. This decreased the predicted current drive magnitude by a factor of 5 and substantially broadened the ECCD profile. Direct evidence for the radial diffusion of the energetic electrons created by EC waves on TCV was found using an energy resolved, multi-chord, hard x-ray pinhole camera [3]. Conversely, experiments on the JT-60U tokamak found that the ECCD profile determined using a motional Stark effect (MSE) diagnostic was in agreement with quasi-linear Fokker-Planck modeling with radial transport turned off [4]. The successful suppression of NTMs on JT-60U using unmodulated ECCD aimed at the magnetic island location also indicated that the driven current was well localized [5].

A well-diagnosed series of ECCD experiments on the DIII-D tokamak allows exploration of the intermediate regime between TCV and JT-60U. Although the plasma confinement on DIII-D is relatively good, it is predicted that the ECCD profile should be noticeably broadened if the current carrying electrons diffuse at rates similar to the heat diffusion rate [2]. Early experiments on DIII-D at low relative power density ($Q_{EC}/n_e^2 < 1$, where Q_{EC} is the ECCD power density in MW/m^3 and n_e is the electron density in units of 10^{19} m^{-3}) and modest electron temperature ($T_e \leq 6 \text{ keV}$) did not find any clear evidence of radial transport as the ECCD profile could be localized between two MSE channels separated by only 0.05 m [6,7]. Detailed comparisons of the width of the ECCD profile determined from MSE signals with the calculated width from the CQL3D quasi-linear Fokker-Planck code [8] placed an upper limit to the diffusion coefficient of $\approx 0.7 \text{ m}^2/\text{s}$ [9]. The same upper limit to the transport rate was obtained by comparing the measured shrinkage of the 2/1 NTM due to ECCD with the modified Rutherford equation [10].

More recent experiments on DIII-D have produced a more definitive result regarding the effect of particle transport on the ECCD profile by investigating the regime of high relative power density ($Q_{EC}/n_e^2 > 1$) and high electron temperature ($T_e \sim 10 \text{ keV}$). At these values of Q_{EC}/n_e^2 , nonlinear effects are calculated to become important [11], and indeed the radiation temperature from electron cyclotron emission (ECE) is found to be anomalously high relative to Thomson scattering, indicating a significant population of non-thermal electrons. The experiments described in this paper show that a diffusion

coefficient of $\approx 0.4 \text{ m}^2/\text{s}$ is needed to model the width and magnitude of the measured ECCD profile for the high Q_{EC}/n_e^2 cases, while low relative power density cases can be modeled with smaller transport rates.

2. High Electron Temperature Plasmas

These DIII-D experiments studied nearly central ECCD in low-density L-mode plasmas. The 110 GHz waves are launched with X-mode polarization and are absorbed at the 2nd harmonic EC resonance near $\rho = 0.13$, where ρ is the normalized toroidal flux coordinate. The wave parallel index of refraction is $N_{\parallel} = \pm 0.23$ for co/counter injection. Neutral beam injection (NBI) during the plasma current ramp up raises T_e and slows the resistive evolution of the current profile, delaying the onset of sawteeth. The ECCD analysis window occurs over an interval of $\geq 0.4 \text{ s}$ during the sawtooth-free phase, as seen in Fig. 1, because MHD-quiescent discharges are needed to determine the driven current profile from the MSE signals using the poloidal flux diffusion equation [12]. During this phase, NBI is reduced to the bare minimum for MSE acquisition to

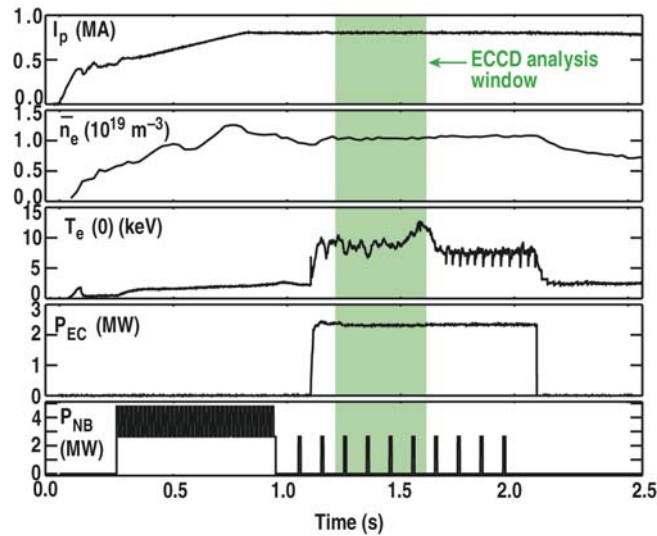


Figure 1. Time history of ECCD discharge 117940 showing use of NBI for preheating and collection of MSE data.

minimize the injection of cold electrons, allowing the highest possible T_e to be achieved. MSE data from identical discharges are sometimes combined together to reduce the experimental uncertainty in the ECCD profile measurement. The noninductive current profile is determined from a time series of magnetic equilibrium reconstructions using Ohm's and Faraday's laws [13,14],

$$\langle \vec{J}_{\text{NI}} \cdot \vec{B} \rangle = \langle \vec{J} \cdot \vec{B} \rangle - \sigma \langle \vec{E} \cdot \vec{B} \rangle, \quad (1)$$

$$\langle \vec{E} \cdot \vec{B} \rangle = F \left\langle \frac{1}{R^2} \right\rangle \left(- \frac{\partial \psi}{\partial t} \Big|_{\rho} - \frac{\rho^2 B_{\phi,0}}{q} \rho_b \frac{d\rho_b}{dt} \right), \quad (2)$$

where J is the current density, E is the electric field, B is the magnetic field, σ is the electrical conductivity, R is the major radius, ρ_b is the effective minor radius, ψ is the poloidal magnetic flux, q is the safety factor, $B_{\phi,0}$ is the vacuum field at the center of the vessel, $F = RB_{\phi}$, and the symbol $\langle \dots \rangle$ denotes the flux surface average.

An anomalously high radiation temperature for the high relative power density cases indicates that a significant population of non-thermal electrons exists. Figure 2 plots the T_e profiles measured by ECE and Thomson scattering for plasmas with $Q_{\text{EC}}/n_e^2 > 2.6$. The (flux surface average) ECCD power density is calculated using the TORAY-GA ray tracing code [15,16]. While fair agreement between these diagnostics is found for radial-injection, the central radiation temperature is ≈ 2 times higher than Thomson scattering for co-injection, and is 3 to 4 times higher for counter-injection (exceeding 20 keV). The high T_e points near the plasma edge from ECE reflect non-thermal emission

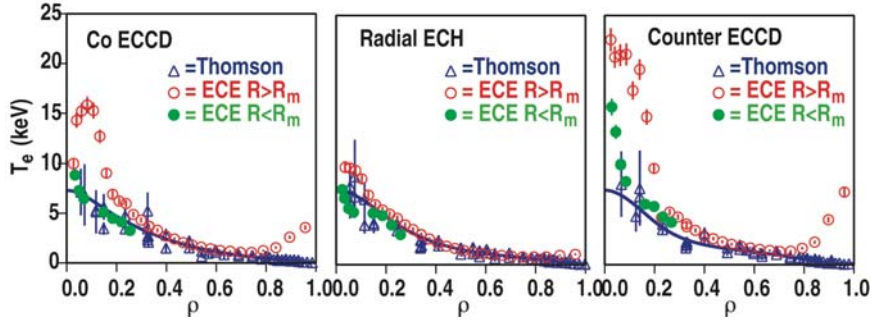


Figure 2. Electron temperature profiles measured by ECE and Thomson scattering for $Q_{\text{EC}}/n_e^2 \geq 2.6$. The mapping of ECE frequency to ρ assumes thermal emission at $2\Omega_e$ to compare to the Thomson data. R_m is the major radius of the magnetic axis.

at the 3rd harmonic on the high field side of the plasma. The absorption and current drive by EC waves is expected to be significantly modified by the non-thermal tail when $Q_{\text{EC}}/n_e^2 > 0.5$ [11]. The CQL3D code indeed predicts significant non-thermal effects for the cases in Fig. 2, most notably flattening of the electron distribution function at low velocities for co/counter injection. A synthetic diagnostic created from the CQL3D output is able to match qualitatively the ECE measurements on DIII-D. The radiation temperature calculated using the CQL3D electron distribution function for counter-ECCD is 4 times higher than the thermal temperature and the modeled ECE profile reproduces the observed high-field-side/low-field-side asymmetry as well.

3. Effect of Particle Transport

These experiments measure a narrow ECCD profile for a single co-injecting gyrotron (injected power $P_{EC} = 0.58$ MW), as seen in Fig. 3. Three additional gyrotrons with radial-injection are used to heat the plasma to maintain a high electron temperature ($T_e = 5.9$ keV) at moderate electron density ($n_e = 3.2 \times 10^{19} \text{ m}^{-3}$). The ECCD profile is determined from the change in the measured noninductive current density in similar plasmas with co-injection and radial-injection. Figure 3 shows that the experimental ECCD profile is in agreement with the CQL3D prediction assuming no radial transport of the electrons. In Fig. 4, the total ECCD measured in the same manner is compared with CQL3D (with radial transport turned off) for plasmas with a variety of conditions ($T_e = 5.9$ -11.3 keV, $n_e = 1.2$ - $3.2 \times 10^{19} \text{ m}^{-3}$, and $P_{EC} = 0.55$ -2.3 MW). This data set extends measurements of ECCD to 70% higher T_e than previously

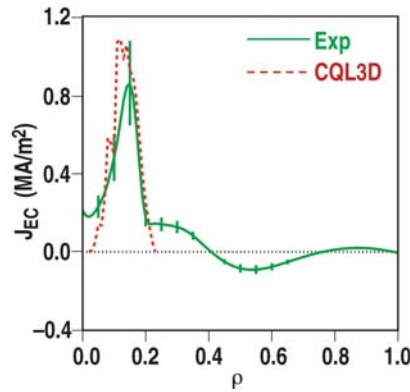


Figure 3. Radial profiles of experimental ECCD and CQL3D modeling for a single gyrotron with $Q_{EC}/n_e^2 = 0.16$.

studied in DIII-D. Good agreement with CQL3D is found for the low relative power density cases ($Q_{EC}/n_e^2 < 0.7$), but for the high relative power density cases ($Q_{EC}/n_e^2 \geq 2.6$) the experimental ECCD falls short of the theoretical expectation. Since the four co-gyrotron injection cases have the same T_e as the one co-gyrotron cases, because in the latter situation three radially-injecting gyrotrons are used to maintain the same temperature, the discrepancy in Fig. 4 at high Q_{EC}/n_e^2 is not due to a problem with the theory at T_e . As previously indicated, for $Q_{EC}/n_e^2 \geq 0.5$ the ECCD efficiency is expected to be power dependent [11], and the ECCD quasi-linear enhancement is $\sim 30\%$ for these plasmas. For convenience, we will use the relative power density as a way of characterizing the ECCD discharges for the remainder of this paper.

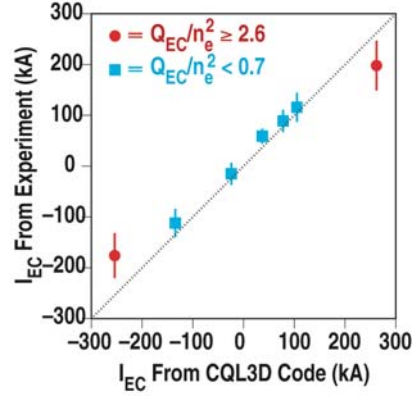
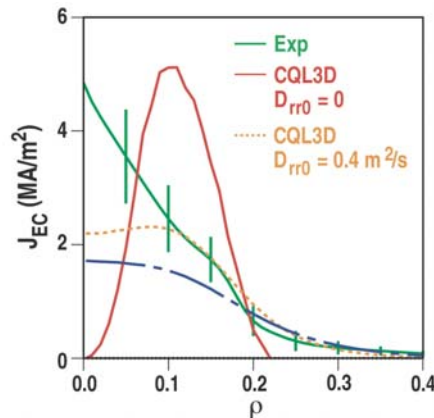


Figure 4. Comparison of experimental and theoretical ECCD magnitudes.

Radial transport of current carrying electrons can explain the lower ECCD for the high relative power density cases. Figure 5 shows that the experimental ECCD profile for the $Q_{EC}/n_e^2 = 2.6$ case with $T_e = 7.9$ keV is clearly lower and broader than the CQL3D prediction assuming no radial transport. To model the effect of electron transport, a radial diffusion operator is used in CQL3D that contains a diffusion coefficient that increases towards the periphery, $D_{rr} = D_{rr0}(1+3\rho^3)[n_{e0}/n_e(\rho)]$, along with a pinch term that is adjusted to maintain a target experimental density profile [2]. At high Q_{EC}/n_e^2 , the total driven current from CQL3D agrees with the measured value (to within the measurement uncertainties) for D_{rr0} between 0.1-1 m^2/s . A tighter constraint can be placed on D_{rr0} by comparing the measured and modeled current densities. Figure 5 shows that $D_{rr0} = 0.4$ m^2/s reproduces well the measured ECCD profile, but $D_{rr0} = 1$ m^2/s produces too broad of a profile. This result is consistent with previous work on DIII-D that determined D_{rr0} must be ≤ 0.7 m^2/s [9,10].

Figure 5. Radial profiles of experimental ECCD and CQL3D modeling for $Q_{EC}/n_e^2 = 2.6$.

This best fit value of $D_{r0} = 0.4 \text{ m}^2/\text{s}$ in Fig. 5 is an order of magnitude less than the electron thermal diffusivity, but it is comparable to the effective particle diffusion coefficient. A radial power balance analysis using the ONETWO transport code [17] coupled to the TORAY-GA ray tracing code [15,16] calculates the electron thermal diffusivity to be $\chi_e \approx 3.7 \text{ m}^2/\text{s}$ just outside the EC wave deposition location. There is greater uncertainty in determining the particle transport rate for these plasmas because the particle source is much smaller than the heat source. However, assuming the particle confinement time is $1 \times$ to $4 \times$ the energy confinement time, the effective (including pinch) particle diffusivity near the ECCD location is calculated to be between $D \sim 0.3 \text{ m}^2/\text{s}$ and $D \sim 0.9 \text{ m}^2/\text{s}$ with a similar radial dependence as D_r used in CQL3D. Thus, the inferred diffusion coefficient of current carrying electrons needed to bring ECCD theory and experiment into agreement is in accordance with the transport rate of thermal particles needed to maintain the density profile (both of which are much less than the heat transport rate). This points out the potential for studying the physics of electron particle transport using precise measurements of the ECCD profile. In effect, the EC waves “tag” superthermal electrons in the plasma at a well-known location, allowing their radial movement to be monitored through the broadening of the current drive profile.

The effect of radial transport is weaker in low relative power density cases, but small amounts of electron diffusion are still possible. As already shown in Fig. 3, a single co-injecting gyrotron at moderate density ($Q_{\text{EC}}/n_e^2 = 0.16$) has an ECCD profile that is consistent with $D_{r0} = 0$. An intermediate case using four co-injecting gyrotrons at moderate density ($Q_{\text{EC}}/n_e^2 = 0.34$) also has a more localized experimental ECCD profile compared to Fig. 5 that is best modeled by CQL3D using $D_{r0} = 0.1\text{-}0.2 \text{ m}^2/\text{s}$. Thus, there is a correlation between the diffusion coefficient of current carrying electrons and the relative power density, perhaps indicating that strongly non-thermal electrons have a higher transport rate than thermal electrons. Future work will try to determine more clearly whether the changes in D_{r0} are a thermal or non-thermal effect.

It is worth mentioning that the total driven current calculated by CQL3D decreases with increasing D_{r0} three times more slowly for high density plasmas than for low density plasmas. This is because the shorter electron slowing down time gives radial transport less time to have an effect.

4. Implications for ECCD on ITER

One of the primary uses of ECCD on ITER will be the suppression of NTM by replacing the “missing” bootstrap current in the magnetic island [1]. The effectiveness of ECCD for this task is strongly dependent of the localization of the noninductive current as a broad current drive profile can make it impossible to stabilize the NTM without modulating the ECCD [18]. First, it should be

noted that the relative power density for ITER will be very small ($Q_{EC}/n_e^2 \ll 0.1$), so total neglect of radial transport effects may be warranted given the DIII-D results discussed in this paper. Second, transport levels will be small on ITER owing to its large size and high plasma current. For example, a simple estimate [2] of the diffusion coefficient for ITER based on the energy confinement time of 3.7 s gives $D_{rr0} = 0.5a^2/4\tau_{E,th} = 0.14 \text{ m}^2/\text{s}$. This may be an overestimate given that $D < \chi_e$ typically. For the case of ECCD aimed at the $q = 2$ surface on ITER, CQL3D modeling (shown in Fig. 6) finds that even particle diffusion coefficients as high as $1 \text{ m}^2/\text{s}$ cause negligible broadening of the current drive profile. Therefore, radial transport will have little effect on the applications of ECCD on ITER.

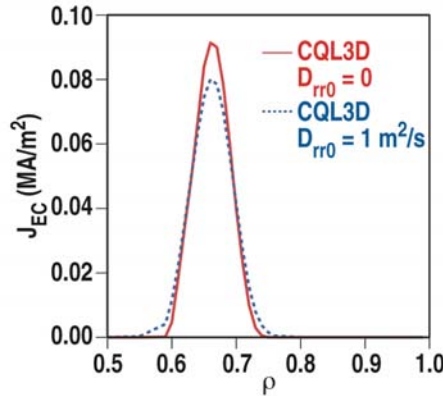


Figure 6. CQL3D modeling of the ECCD profile on ITER.

5. Summary

Up to 200 kA of ECCD has been measured on DIII-D in low-density L-mode plasmas with $T_e \sim 10 \text{ keV}$. These experiments studied the high relative power density regime ($Q_{EC}/n_e^2 > 1$) where the radiation temperature from ECE can exceed 20 keV, indicating a significant population of non-thermal electrons. At low relative power density ($Q_{EC}/n_e^2 = 0.16$), the ECCD profile determined by MSE polarimetry agrees with the CQL3D quasi-linear Fokker-Planck code with radial transport turned off. However, at high relative power density ($Q_{EC}/n_e^2 = 2.6$), the measured ECCD profile is noticeably reduced and broadened, demonstrating that radial diffusion of the current carrying electrons is not negligible. A particle diffusion coefficient of $\approx 0.4 \text{ m}^2/\text{s}$ is required in CQL3D to reproduce the experimental ECCD profile for this latter case, but smaller diffusion coefficients are needed to model the ECCD profile at intermediate Q_{EC}/n_e^2 values. This level of transport is an order of magnitude less than the electron thermal diffusivity for these plasmas, but it is comparable to the effective particle diffusion coefficient needed to maintain the density profile. Fortunately,

this level of particle diffusion should have little effect on the application of ECCD to ITER, and total neglect of radial transport may even be warranted given the very low relative power density on ITER ($Q_{EC}/n_e^2 \ll 0.1$).

References

1. T. C. Hender *et al.*, *Nucl. Fusion* **47**, S128 (2007).
2. R. W. Harvey *et al.*, *Phys. Rev. Lett.* **88**, 205001 (2002).
3. T. P. Goodman *et al.*, in *Proc. 19th Int. Conf. on Fusion Energy 2002*, Lyon (IAEA, Vienna, 2002), OV/4-2 (CD-ROM).
4. T. Suzuki *et al.*, *Nucl. Fusion* **44**, 699 (2004).
5. A. Isayama *et al.*, *Plasma Phys. Control. Fusion* **42**, L37 (2000).
6. C. C. Petty *et al.*, *Nucl. Fusion* **41**, 551 (2001).
7. C. C. Petty *et al.*, *Nucl. Fusion* **42**, 1366 (2002).
8. R. W. Harvey and M. G. McCoy, in *Proc. IAEA Tech. Comm. Meet. 1992* (IAEA, Vienna, 1993), p. 498.
9. C. C. Petty *et al.*, *Nucl. Fusion* **43**, 700 (2003).
10. C. C. Petty *et al.*, in *Proc. 15th Top. Conf. Radio Frequency Power in Plasmas, 2003*, Moran (AIP, New York, 2003), p. 348.
11. R. W. Harvey *et al.*, *Phys. Rev. Lett.* **62**, 426 (1989).
12. C. C. Petty *et al.*, in *Proc. 13th Joint Workshop on ECE and ECH, 2004*, Nizhny Novgorod (RAS, Nizhny Novgorod, 2005), p. 189.
13. C. B. Forest *et al.*, *Phys. Rev. Lett.* **73**, 2444 (1994).
14. L. L. Lao *et al.*, in *Proc. 14th Top. Conf. Radio Frequency Power in Plasmas, 2001*, Oxnard (AIP, New York, 2001), p. 310.
15. K. Matsuda, *IEEE Trans. Plasma* **17**, 6 (1989).
16. Y.-R. Lin-Liu *et al.*, in *Proc. Euro. Conf. on Controlled Fusion and Plasma Physics, 1999*, Maastricht (EPS, Geneva, 1999), Vol. 23J, p. 1245.
17. H. St John *et al.*, in *Proc. 15th Int. Conf. on Plasma Physics and Controlled Nuclear Fusion Research 1994*, Seville (IAEA, Vienna, 1995), Vol. 3, p. 603.
18. R. Prater *et al.*, *Nucl. Fusion* **43**, 1128 (2003).